Deep learning for space-borne focal-plane wavefront sensing

Maxime Dumont, Carlos Correia, Jean-François Sauvage,

Noah Schwartz, Morgan Gray, et al.

Published version information:

Citation: M Dumont et al. Deep learning for space-borne focal-plane wavefront sensing. Proc SPIE 12180 (2022): 1218034. Is in proceedings of: Space Telescopes and Instrumentation 2022: Optical, Infrared, and Millimeter Wave, Montréal, Québec, Canada, 17-23 Jul 2022.

DOI: 10.1117/12.2628868

PROCEEDINGS OF SPIE

SPIEDigitalLibrary.org/conference-proceedings-of-spie

Deep learning for space-borne focal-plane wavefront sensing

Maxime Dumont, Carlos Correia, Jean-François Sauvage, Noah Schwartz, Morgan Gray, et al.

Maxime Dumont, Carlos Correia, Jean-François Sauvage, Noah Schwartz, Morgan Gray, Olivier Beltramo-Martin, Jaime Cardoso, "Deep learning for space-borne focal-plane wavefront sensing," Proc. SPIE 12180, Space Telescopes and Instrumentation 2022: Optical, Infrared, and Millimeter Wave, 1218034 (27 August 2022); doi: 10.1117/12.2628868

SPIE.

Event: SPIE Astronomical Telescopes + Instrumentation, 2022, Montréal, Québec, Canada

Deep learning for space-borne focal-plane wavefront sensing

DUMONT Maxime[1,2,3], CORREIA Carlos[2,4], SAUVAGE Jean-François[1,3], SCHWARTZ Noah[5], GRAY Morgan[3], BELTRAMO-MARTIN Olivier[6], and CARDOSO Jaime[2]

[1]DOTA, ONERA, F-13661 Salon Cedex Air - France
[2]INESCTEC, FEUP, Porto, Portugal
[3]Aix-Marseille Université, CNRS, CNES, LAM, Marseille, France
[4]SPACE ODT, Porto, Portugal
[5]UK Astronomy Technology Centre, Edinburgh, EH9 3HJ United Kingdom
[6]SpaceAble, Paris, France

ABSTRACT

For space-based Earth Observations and solar system observations, obtaining both high revisit rates (using a constellation of small platforms) and high angular resolution (using large optics and therefore a large platform) is an asset for many applications. Unfortunately, they prevent the occurrence of each other. A deployable satellite concept has been suggested that could grant both assets by producing jointly high revisit rates and high angular resolution of roughly 1 meter on the ground.
This concept relies however on the capacity to maintain the phasing of the segments at a sufficient precision (a few tens of nanometers at visible wavelengths), while undergoing strong and dynamic thermal gradients. In the constrained volume environment of a CubeSat, the system must reuse the scientific images to measure the phasing errors.
We address in this paper the key issue of focal-plane wave-front sensing for a segmented pupil using a single image with deep learning. We show a first demonstration of measurement on a point source.
The neural network is able to identify properly the phase piston-tip-tilt coefficients below the limit of 15nm per petal.

Keywords: Wavefront sensing, Focal plane wavefront sensing, Deep learning, Neural Network, Artificial Intelligence, Astronomy, Nanosatellite, CubeSat

1. INTRODUCTION

For Earth and planet observation, obtaining high revisit rates commonly implies the use of a constellation of satellites which in turn means the use of affordable and small platforms. On the other hand, high angular resolution requires large apertures.
In this paper we advance this paradigm by analysing wavefront sensing options onboard a deployable telescope in a nanosatellite (CubeSat standard [1]). This deployable telescope, whose pupil diameter is about 30cm, is very sensitive to the wavefront quality and thus to the good primary mirror co-phasing. Due to its miniaturised nature, only focal-plane data is likely accessible.
Obtaining a diffraction-limited imagery and provide about 1 meter resolution from Low Earth Orbit [LEO] requires a good wavefront quality. We define this required quality around 50-70nm at visible wavelengths (meaning roughly $15nm$ per petal). As no additional optics is integrable in such a small platform, a direct focal plane image analysis is proposed to identify the wavefront aberrations using a NN whose internal parameters are taught using a data-driven learning procedure.
Wavefront sensing using deep learning has been proposed several times in the literature, especially by combining phase diversity and deep learning [2,3], others use deep learning to retrieve non common path aberrations [4]. Retrieving phase aberrations with one single image has been done with the Inception v3 network, in the work of Paine and Fienup [5].
In our conceptual configuration, performing wavefront sensing with the particular pupil shape and the few degrees of freedom complicates the problem. The primary mirror of the suggested configuration would be composed by 4 independent square mirrors (10cm*10cm) below which are 3 actuators, allowing the correction of the 4 petals in

Space Telescopes and Instrumentation 2022: Optical, Infrared, and Millimeter Wave, edited by Laura E. Coyle, Shuji Matsuura, Marshall D. Perrin, Proc. of SPIE Vol. 12180, 1218034 · © 2022 SPIE · 0277-786X · doi: 10.1117/12.2628868

piston tip and tilt. These 12 parametric coefficients are those the neural network needs to identify from the focal plane image. The optimal performance to reach is the diffraction limit which corresponds (when considering each petal individually) to a WaveFront Error [WFE] of 15nm per petal meaning around $60nm$ over the full pupil.

2. FROM IMAGE FORMATION TO DEEP LEARNING

In order to reduce the complexity of the problem, a point source is studied here. Further work will focus on extended scenes from the Earth surface.

Studying the point source case allow us to work directly with the system Point Spread Function [PSF]. The PSF describes the light distribution in the focal plane of an optical system observing a point source, as an unresolved star. Its shape is a function of the wavefront aberration; therefore we are trying to recover the phase information given a measurement of the PSF. Figure 1 shows the PSF for a segmented pupil with the particular shape under study. This PSF result from the interference in the pupil plane between the 4 petal's electric field.

$$\text{PSF} = |\text{FT}(Ae^{j\phi})|^2 \text{ where } \phi = \frac{2j\pi\text{OPD}}{\lambda} \tag{1}$$

Where FT is the Fourier transformation, A is the amplitude of the pupil electric field, ϕ the phase of the pupil electric field and OPD is the Optical Path Difference image.

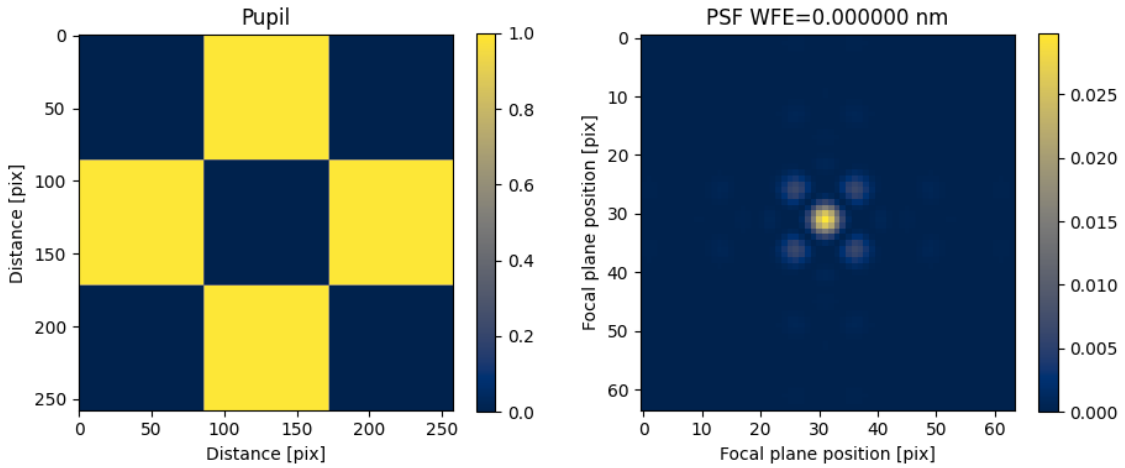

Figure 1. Segmented pupil (left) and corresponding PSF (right)

The PSF can be described with the Optical Path Difference [OPD] function as in Eq.1 . Here, we define the OPD using the Zernike basis. Due to the miniaturization of the telescope, 3 actuators are used to control each petal. It allows the correction of these petals for the 3 first Zernike modes only: Piston, Tip and Tilt. Therefore, the wavefront can be corrected using 12 coefficient (3*4petals). The Wavefront Error [WFE], representing the residual wavefront after correction, is defined using these 12 coefficients. As shows Fig.2, the phase aberrations disturb the PSF hence the image.
Since the global piston over the full pupil has no impact on imaging, we filter out the mean piston by computing Eq.2 on the coefficient vector p:

$$p' = (I - \begin{bmatrix}1\\1\\1\\1\end{bmatrix} * \begin{bmatrix}\frac{1}{4} & \frac{1}{4} & \frac{1}{4} & \frac{1}{4}\end{bmatrix}) * p \tag{2}$$

where p is the vector of the 4 piston coefficients and p' the new piston vector. Note the global-piston-removing matrix rank in Eq.2 is 3.
Once done, the OPD is generated from the 12 coefficients and then the corresponding aberrated PSF is computed using Eq.1 as shown in Fig.2.

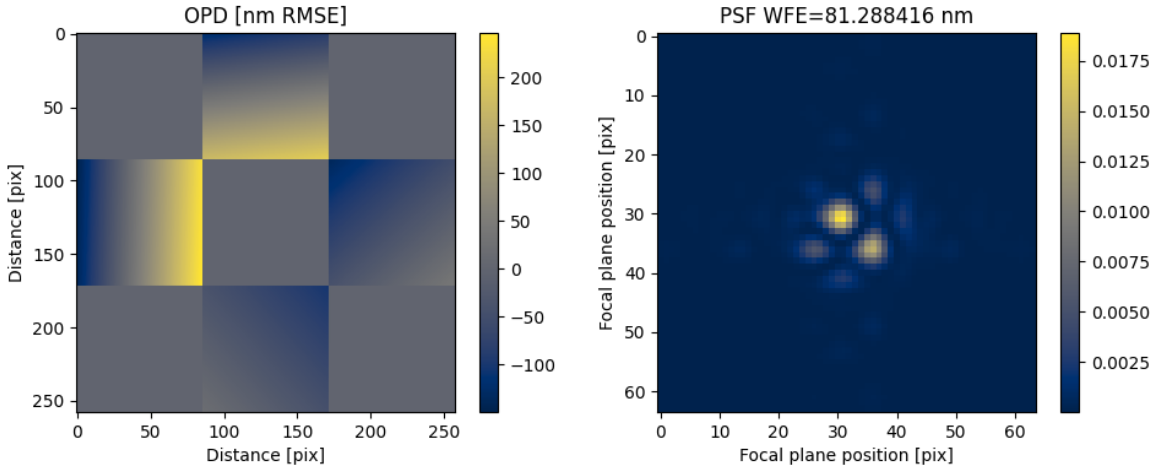

Figure 2. Aberrated OPD (left) and corresponding PSF (right)

Moreover, due to the segmented nature of the pupil with disjoint segments, the variance is independent between each petal. Thus, the associated WFE is computed with the linear sum over each petal of the quadratic sum over each mode:

$$WFE = \sum_{petal=1}^{4} \sqrt{\sum_{mode=1}^{3} c^2_{petal,mode}} \tag{3}$$

Once the data generated, the input (or initial) WFE follows a Gaussian distribution centered in $4\sqrt{3} * \sigma$ when σ is the aberration for each coefficient, and is chosen the same for all 12 coefficients. This generation method is used to produce a **training dataset** of 10^5 PSFs, dedicated to the neural network training. Another set of PSFs is created with different draws of coefficients (but with same distribution) to create the **testset** in order to test the neural network accuracy in estimating the corresponding piston-tip-tilt coefficients on each petal.

3. METHOD

3.1 Training and sign ambiguity

The training of the Neural network requires a huge amount of data to be representative of the input coefficients and adjust the neural network internal parameters. 10^5 PSFs are generated following the distribution shown in Fig.3.

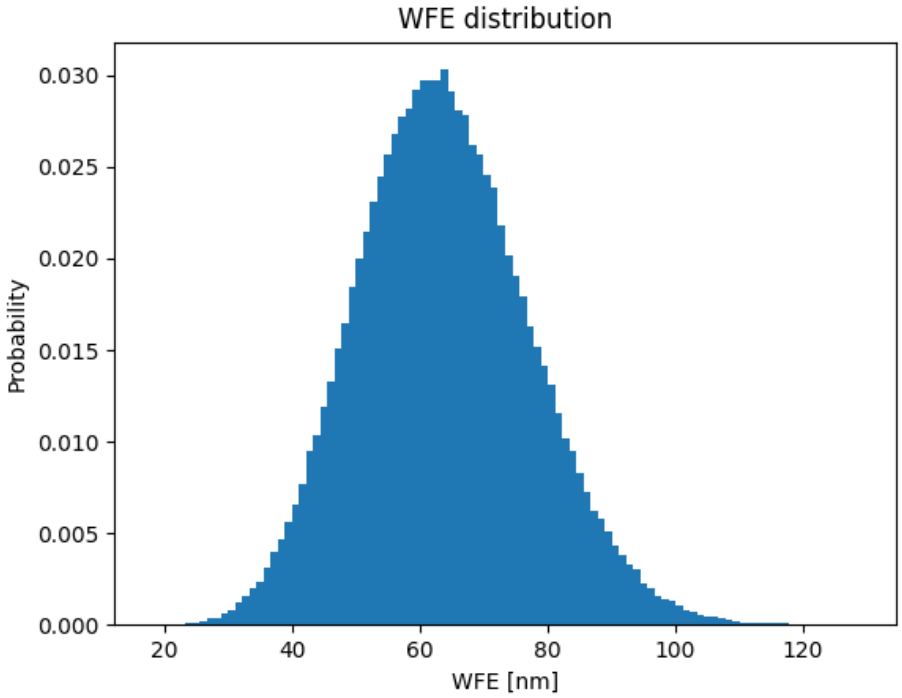

Figure 3. WFE distribution for the training set and test set.

This distribution corresponds to the initial WFE over the full pupil with $\sigma = 9nm$ for all 12 coefficients.
A VGG-net like architecture is used here over 150 epochs with a constant learning rate about $5e^{-5}$ and a batch size of 32 PSFs. During the training, a loss function is used to estimate the precision of the estimation of the neural network. The most common loss function is the RMSE : $Loss_{RMSE} = \sqrt{\frac{1}{12}\sum_{i=1}^{12}(c_i - \hat{c_i})^2}$. It represents the square root of the mean of the quadratic error for each phase coefficient directly. It a good indicator to appreciate how far the NN is from the estimation of each coefficient during the training. The $Loss_{RMSE}$ is only computed for the NN training and represents the mean error per coefficient; in order to analyse the NN estimation, the WFE in Eq. 3 is used. The WFE allows the optical appreciation of the full pupil wave front estimation quality once the training done. It also can be used as a loss function in further study but it's not the case here.
The validation loss is the loss function computed on the data that are not seeing during the training process after each step of the training (named epoch). At the last step, the validation loss converge at $Loss_{RMSE_{Val}} = 30nm$ in average . This $Loss_{RMSE_{val}}$ value is insufficient for a proper wavefront analysis (we would like the precision accuracy to be much better than the required 15nm per petal, and with 30nm per coefficient the estimation is widely out of bound), but is clearly explained when analysing the error of WFE between odd and even phasemaps :
Using the 1000 PSFs from the test set, we compute the WFE and by splitting the even and odd part of the estimated wavefront map, we can notice the difficulty of the neural network to identify the even part of the phase as illustrated in Fig.4.

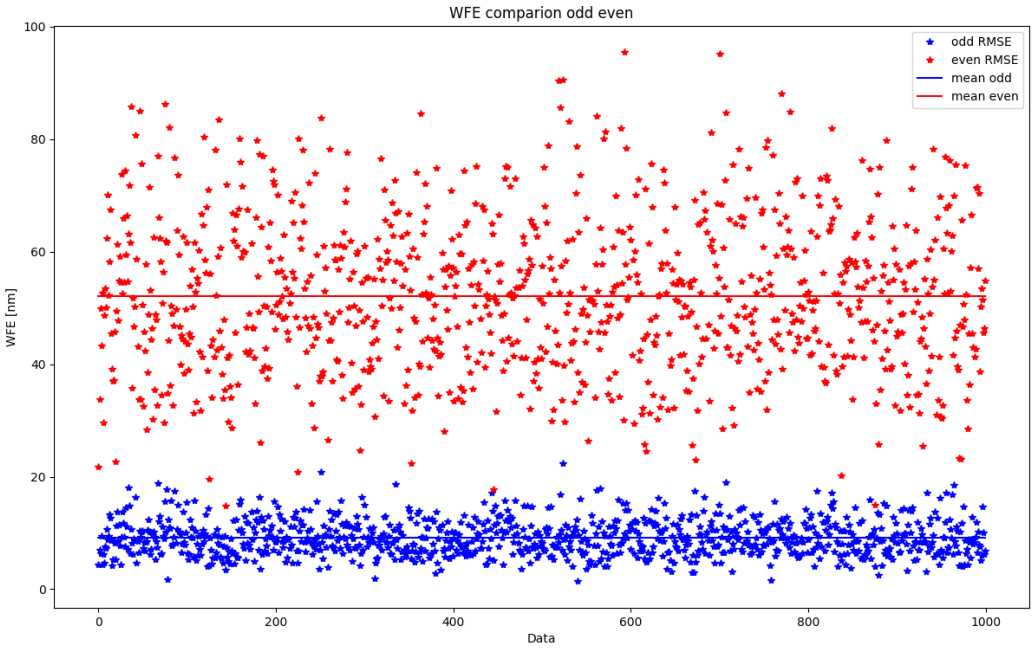

Figure 4. Neural network estimation WFE on even (red) and odd (blue) part of the phase map

This is due to the centrosymetry of the pupil. This error is well-known, and is called the sign ambiguity, this result was therefore fully expected. This error is intrinsic to image formation, and any focal-plane wavefront sensor would be insensitive to it: a single even mode can generate similar PSFs and therefore the NN cannot overcome this ambiguity. To overcome this issue, we need either to add diversity to the image formation (by using an additional defocused image), or to break the symmetry of the pupil. As the purpose of this work is to use one single image from the focal plane, we choose the second solution: we crop 10% of the segment's corner for two of the four petals in order to break the pupil's symmetry. The PSF has his shape modified (see Fig.5) and we can generate 10^5 data and train another NN with the asymetric pupil. Then computing the same process as above we obtain the odd and even WFE corresponding Fig.6.

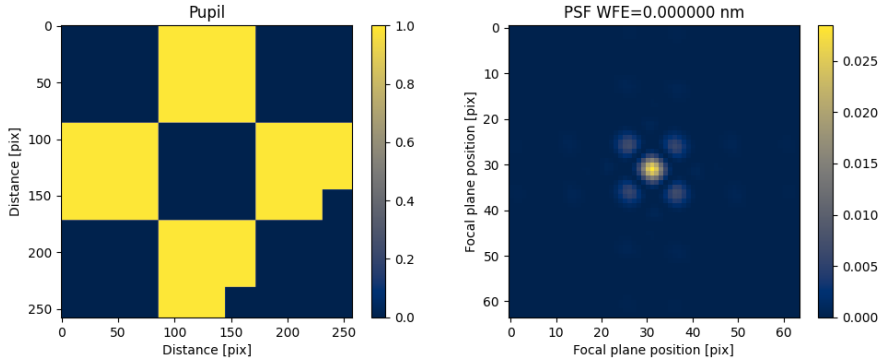

Figure 5. Asymetric pupil and corresponding PSF

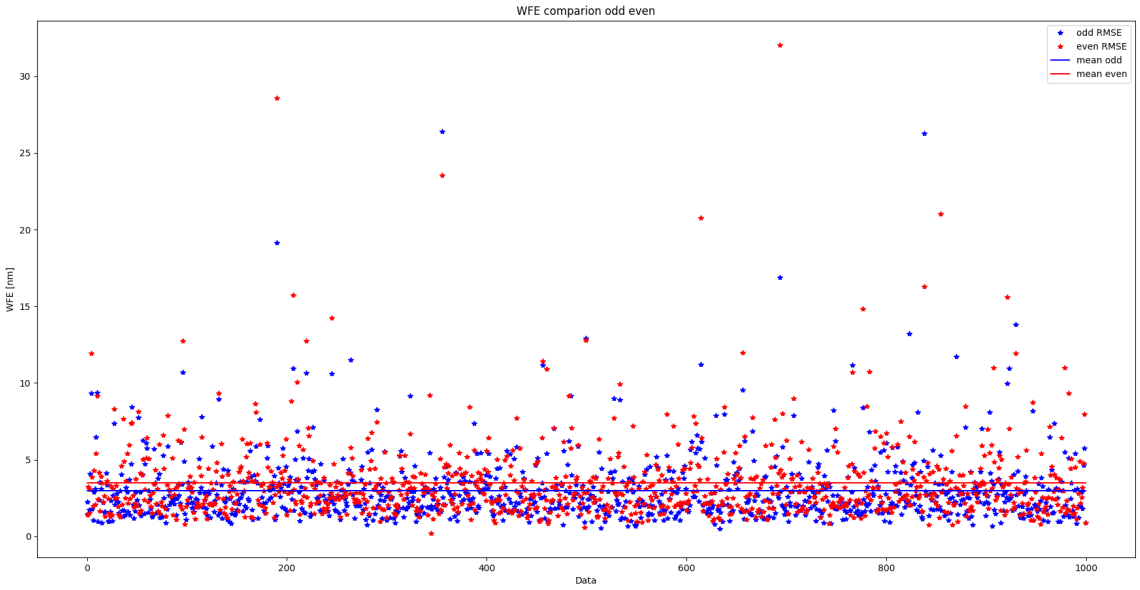

Figure 6. Neural network estimation WFE on even (red) and odd (blue) part of the phase map with amplitude diversity

Fig 6 shows the impact of the asymmetric pupil and the improvement in the estimation of the even part of the phase. The WFE on the even part of the phase decreases from 42 nm RMS to 3nm RMS with the asymmetric pupil. The neural network makes an accurate estimation of the phase from the focal plane image.

3.2 NN performance

The asymmetric pupil allows a better wavefront analysis and boosts the NN performance, see Fig.7.

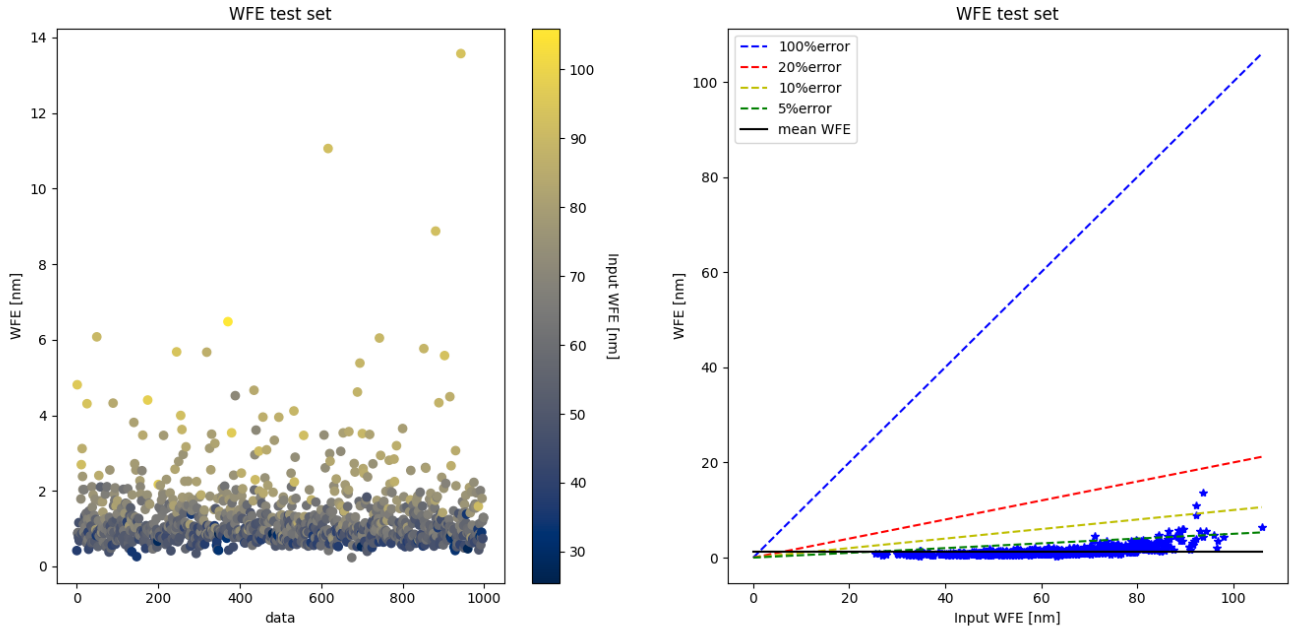

Figure 7. Neural network estimation WFE (left) and comparison with the initial WFE (right)

The NN estimation is accurate for a small wavefront. It is able to recover about 95% of the WFE. The mean WFE for the estimation is around 3nm RMS which is significantly under the expected performance. We can notice that a few cases present a WFE around 10 nm rms. These cases correspond to input WFEs around 100nm, a value that has been barely seen during the NN training range. It shows that the NN is able to generalize the non linear problem even if the input WFE is hardly in the aberrations training range. It is therefore able to reduce the initial WFE by a factor 10.

4. CONCLUSION

We have demonstrated a NN-based algorithm able to estimate the 12 coefficients of phasing of a deployable telescope onboard a CubeSat from a single in-focus point-source focal-plane image using an asymmetric pupil (amplitude diversity). This method however, can be applied to any non-space telescope as well. This ML-based focal plane wavefront sensing method has shown good performance in the case of a segmented pupil observing a point source. Without the presence of noise, the residual can be further reduced by implementing the neural network in a closed loop. Further work will focus on using noisy data and a closed loop. The results will be compared to wavefront sensing with classical phase diversity in terms of performance and computational burden.

5. ACKNOWLEDGMENTS

This work is supported by European Structural and Investment Funds in the FEDER component, through the Operational Competitiveness and Internationalization Programme (COMPETE 2020) [Project nº 047264; Funding Reference: POCI-01-0247-FEDER-047264]. Authors are acknowledging the support by the Action Spécifique Haute Résolution Angulaire (ASHRA) of CNRS/INSU co-funded by CNES. This project is supported by ANR WOLF.

REFERENCES

[1] Schwartz, N., Brzozowski, W., Milanova, M., Morris, K., Todd, S., Ali, Z., Sauvage, J.-F., Ward, A., Lunney, D., and Macleod, D., "High- resolution deployable cubesat prototype," in [*Space Telescopes and Instrumentation 2020: Optical, In- frared, and Millimeter Wave, Dec 2020, Online Only, United States*], 96 (2020).

[2] Nishizaki, Y., Valdivia, M., Horisaki, R., Kitaguchi, K., Saito, M., Tanida, J., and Vera, E., [*Deep learning wavefront sensing*], Opt. Express 27, New York.

[3] Andersen, T. E., Owner-Petersen, M., and Enmark, A., [*Image-based wavefront sensing for astronomy using neural networks*], J. Astron. Telesc. Instrum. Syst. 6(3) (2020).

[4] de Xivry, G. O., Quesnel, M., Vanberg, P.-O., Absil, O., and Louppe, G., [*Focal plane wavefront sensing using machine learning: performance of convolutional neural networks compared to fundamental limits*], MNRAS, second ed. (2021).

[5] Paine, S. W. and Fienup, J. R., "Machine learning for improved image-based wavefront sensing," in [*Opt. Lett. 43*], 1235–1238 (2018).